Repurposing Inactive Oil and Gas Wells for Energy Storage: Maximizing the Potential Via Optimal Drivetrain Control

Preprint

Shubham Sundeep,[1] Latha Sethuraman,[1] Dayo Akindipe,[1] Lee Fingersh,[1] Zach Wenrick,[2] and Aaron Munoz[2]

1 National Renewable Energy Laboratory
2 Renewell Energy

Presented at the 12th International Conference on Power Electronics, Machines and Drives (PEMD)
Brussels, Belgium
October 23–24, 2023

NREL is a national laboratory of the U.S. Department of Energy
Office of Energy Efficiency & Renewable Energy
Operated by the Alliance for Sustainable Energy, LLC

This report is available at no cost from the National Renewable Energy Laboratory (NREL) at www.nrel.gov/publications.

Contract No. DE-AC36-08GO28308

Conference Paper
NREL/CP-5000-86579
January 2024

Repurposing Inactive Oil and Gas Wells for Energy Storage: Maximizing the Potential Via Optimal Drivetrain Control

Preprint

Shubham Sundeep,[1] Latha Sethuraman,[1] Dayo Akindipe,[1] Lee Fingersh,[1] Zach Wenrick, and [2] Aaron Munoz[2]

1 National Renewable Energy Laboratory
2 Renewell Energy

Suggested Citation
Sundeep, Shubham, Latha Sethuraman, Dayo Akindipe, Lee Fingersh, Zach Wenrick, Aaron Munoz. 2024. *Repurposing Inactive Oil and Gas Wells for Energy Storage: Maximizing the Potential Via Optimal Drivetrain Control: Preprint*. Golden, CO: National Renewable Energy Laboratory. NREL/CP-5000-86579.
https://www.nrel.gov/docs/fy24osti/86579.pdf.

NREL is a national laboratory of the U.S. Department of Energy
Office of Energy Efficiency & Renewable Energy
Operated by the Alliance for Sustainable Energy, LLC

This report is available at no cost from the National Renewable Energy Laboratory (NREL) at www.nrel.gov/publications.

Contract No. DE-AC36-08GO28308

Conference Paper
NREL/CP-5000-86579
January 2024

National Renewable Energy Laboratory
15013 Denver West Parkway
Golden, CO 80401
303-275-3000 • www.nrel.gov

NOTICE

This work was authored in part by the National Renewable Energy Laboratory, operated by Alliance for Sustainable Energy, LLC, for the U.S. Department of Energy (DOE) under Contract No. DE-AC36-08GO28308. Funding provided by the U.S. Department of Energy Office of Energy Efficiency and Renewable Energy Wind Energy Technologies Office. The views expressed herein do not necessarily represent the views of the DOE or the U.S. Government. The U.S. Government retains and the publisher, by accepting the article for publication, acknowledges that the U.S. Government retains a nonexclusive, paid-up, irrevocable, worldwide license to publish or reproduce the published form of this work, or allow others to do so, for U.S. Government purposes.

REPURPOSING INACTIVE OIL AND GAS WELLS FOR ENERGY STORAGE: MAXIMIZING THE POTENTIAL VIA OPTIMAL DRIVETRAIN CONTROL

Shubham Sundeep*^, Latha Sethuraman*, Dayo Akindipe*, Lee Fingersh*, Zach Wenrick+, Aaron Munoz+

*National Renewable Energy Laboratory, Denver, Colorado, USA
+Renewell Energy, Bakersfield, California, USA
^shubham.sundeep@nrel.gov

Keywords: GRAVITY ENERGY STORAGE, PERMANENT MAGNET SYNCHRONOUS MOTOR, PWM CONVERTER, MAXIMUM TORQUE PER AMPERE CONTROL.

Abstract

In recent years, there has been a growing emphasis on utilizing energy storage to enhance grid resilience against disruptive events. While renewable energy supply continues to expand, gravity-based solutions like pumped hydro remain dominant in the commercial space. However, their geographical limitations constrain availability, scalability, and increase costs for co-locating solar and wind energy. An alternative approach proposes repurposing idle oil and gas wells located closer to existing grid infrastructure, offering a promising and cost-effective solution. This paper addresses the optimization and control of a regenerative drive system coupled to an interior permanent magnet synchronous machine in a 300-meter well with a 100-Newton weight. The study employs a dynamic MATLAB/Simulink model to simulate the operation of the electric drivetrain system during storage and discharge operations. The results demonstrate an initial round-trip efficiency of 85.9% for the electrical system alone and identify crucial factors for maximizing efficiency. The optimized operation and control of the electromechanical drivetrain system hold great potential for minimizing the levelized cost of storage while maximizing efficiency and revenue generation.

1. Introduction

Renewables are projected to increase from their current share of 12% of the global energy supply to 90% in 2050 [1]. However, their intermittent nature necessitates increased storage, as the existing power system continues to be vulnerable to extreme weather events and cyber-physical attacks. In the commercial space, global energy storage capacity is dominated by gravity-based pumped hydro, with the remaining contributions coming from flow batteries, compressed air, flywheels, and other gravity-based mechanical systems. However, these systems are challenged by carbon-intense construction, the cost of co-locating solar and wind, and low round-trip energy efficiency (70%).

Repurposing the numerous idle and orphaned oil and gas wells that are conveniently located closer to existing grid infrastructure offers a promising low-cost solution. Idle and orphaned oil wells belong to the category of wells that are no longer economically feasible for oil and gas production or extraction. They may be repurposed for activities such as natural gas storage, waste fluid disposal, or monitoring. However, failure to adequately monitor and maintain wells can result in the severe degradation of isolation materials such as cement and casings, transforming them into pathways for gas migration to the surface. This contributes to harmful methane emissions and can pose environmental risks to communities and ecosystems. [2]. According to a recent report by The Interstate Oil and Gas Compact Commission (IOGCC), as of 2020, 1,619,071 idle wells exist in U.S.A. territories [2]. At least 92,198 of these wells are orphaned. Each of these wells is about 8 inches in diameter and has a depth in the range of 150 m to 3000 km. The prevalence of these wells presents a significant challenge, prompting innovative solutions to utilize their potential for other beneficial applications.

Idle wells near the existing grid can be converted into utility-scale gravity energy storage systems (GESSs). GESSs store energy by lifting weights through height, enabling the capture and release of surplus energy from renewables. The depth and dimensions of abandoned wells make them ideal for energy harvesting through GESSs, offering benefits such as no additional infrastructure, quick power balancing response, grid resilience, flexible storage scheduling, adaptation to electricity demand, coverage for renewable energy fluctuations, rapid demand response, voltage stability, power factor correction, and grid stabilization support.

The economic viability of such GESS based on repurposed oil well infrastructure will depend on the levelized cost of storage (LCOS), which considers the economic and technical parameters that influence lifetime, the cost of storing and discharging energy, and the round-trip efficiency. The round-trip efficiency is the ratio of energy stored to energy retrieved in a system. It is an important factor, as higher efficiency translates to reduced losses and improved profitability. Efforts are currently being made to achieve high round-trip efficiency.

The electromechanical drivetrain system encompassing the motor, gearbox, and inverter plays a crucial role in controlling weight ramp rates and energy storage capacity, thus impacting the round-trip efficiency. Minimizing the losses in this system will maximizes the round-trip efficiency.

Requirements for power quality (IEEE standards [3,4]) have made most GESS designers select variable-speed AC motors with regenerative abilities and power converters that can accommodate gradual acceleration and deceleration during charging and discharging. Botha et al. [5] focused on the optimal selection of drivetrain candidates for GESS considering the use of permanent magnet-based synchronous machines for higher drivetrain efficiency. Ana et al. [6] explored the use of high-speed permanent magnet motors for small-scale industrial GESS Studies using conventional wound rotor synchronous machines and asynchronous machines (squirrel cage and wound rotor) have been reported [7,8]. Although the choice of motor and inverter system is determined by several factors, including costs, overload capability, and efficiency, induction motors have been known to be the most cost competitive solution with the shortest lead times and greatest availability. Published reports on the operation and control of the electromechanical system have been very limited and have focused on hybrid GESS driven by induction motors [7].

Gravitricity [9] are exploring the potential of GESS in abandoned coal mines using high-speed induction motors. Their studies found that increasing the weight's mass or density improves storage capacity, but with diminishing returns. Motor and converter capacity limit the ramp rate, highlighting the need for efficient selection to maximize round-trip efficiency. Another company, Gravity Power [10] drills boreholes, pressurizing water for storage, wherein a reversible pump turbine with a conventional motor/generator lifts a piston. This system is an evolved pumped-storage hydro system that achieves a round-trip efficiency of around 70%. Tong et al. [7] and Loudiyi et al. [11] modeled a pumped-hydro storage GESS with a conventional synchronous generator. They observed significant oscillations in stator current, excitation voltage, and generated power during load variations, which indicates need of an optimized Proportional-Integral-Derivative (PID) controller.

More recently, Renewell Energy [12] has been at the forefront of repurposing idle wells for GESS. Their approach involves first sealing the wells just above the production zone, which effectively mitigates the methane gas emissions and prevents toxic fluids from leaching into nearby water resources. Utilizing an electromechanical drivetrain system, they then raise and lower weights into these wells to store and discharge energy from and to the grid. The development of the system is supported by the National Renewable Energy Laboratory (NREL) and funded by the Advanced Research Program Agency-Energy (ARPA-E) RIGS-UP project [13]. NREL's involvement ensures selection and operation of optimal drivetrain to maximize the round-trip efficiency As part of this effort, this study demonstrates optimal control and operation of a regenerative motor-drive unit with a 30-hp high-speed interior permanent magnet synchronous machine (IPMSM) using a MATLAB/Simulink model. IPMSMs offer several advantages, including high efficiency and torque, compactness, precise control, reliability, and low maintenance requirements, making them highly suitable for the RIGS-UP GESS.

This paper is structured as follows. Section 2 describes the basic principle of the RIGS-UP GESS. Section 3 describes the control and operation of the IPMSM drive along with the pulse width modulated (PWM) converter, including the maximum torque per ampere (MTPA) method [15]. In Section 4, the proposed control is validated, and in Section 5, concluding remarks are made.

2. The RIGS-UP Gravity Energy Storage System (GESS)

The basic principle of the RIGS-UP GESS is similar to that of many conventional GESS systems. It uses an available depth or gradient to store the surplus energy from nonconventional sources, except the depth is filled with an incompressible fluid. The energy is stored in the form of potential energy (E) using a certain mass m, suspended at a depth h, which is expressed as [5–7]:

$$E\ (J) = mgh, \tag{1}$$

where g is the acceleration due to gravity. This energy can be expressed in kWh as [3–5]:

$$E\ (kWh) = (2.77 \times 10^{-7}) \times mgh. \tag{2}$$

During periods of surplus power, a motor-drive system raises the weight through a height h, thereby converting the electrical energy into mechanical potential energy. The movement of the weight is resisted by the hydrodynamic drag and buoyant force from the surrounding fluid. During storage, which typically lasts for several hours to a few days, the weight is suspended. When the electricity demand exceeds the generation, the electromechanical system lowers the weight and converts the potential energy into electrical energy. Fig. 1 shows a schematic diagram of the RIGS-UP GESS, wherein a cylindrical weight of mass m, diameter d, and density ρ is suspended in a well shaft of depth D. The major components

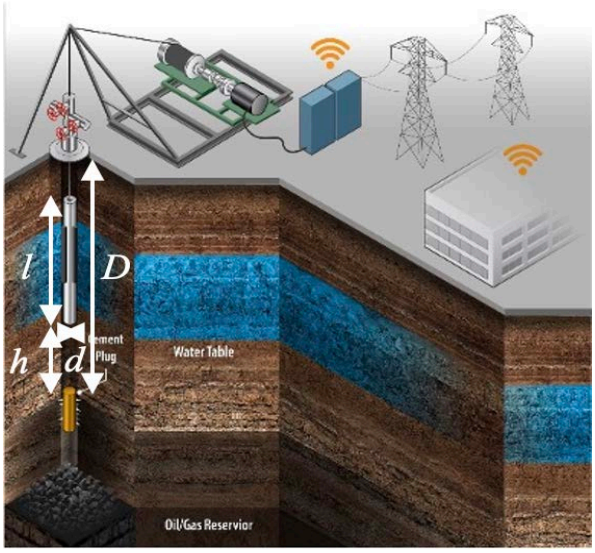

Fig. 1. Schematic of the RIGS-UP gravity energy storage system.

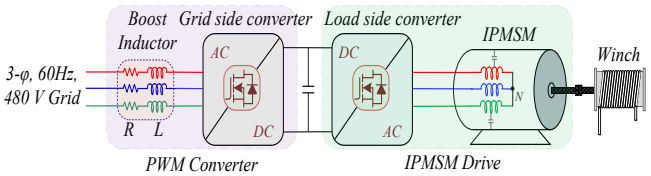

Fig. 2. Schematic of the power electronics system comprising an IPMSM fed through a PWM converter.

of this system are (1) the well shaft, (2) the suspended weight, and (3) the electromechanical system, which raises and lowers the weight in the well shaft. This electromechanical system is crucial in the lifting mechanism, which consists of a winch and a wire drum connected to an electrical machine through a gearbox. The grid provides the necessary power to drive the winch, while the gearbox converts the rotational motion of the machine into a suitable torque and lower speed for the drum. The machine connected to the winch plays a vital role in power conversion, converting electrical energy from the grid into rotational mechanical energy during charging. The winch then converts this mechanical energy into linear motion, storing it as potential energy. During discharge, the process is reversed, with the machine converting the mechanical energy back into electrical energy. Therefore, efficient electromechanical power conversion is essential for achieving the highest round-trip efficiency.

2.1 Drivetrain Schematic, Specifications, and Assumptions

In this study, we explore the performance of a high-speed IPMSM in motoring and regeneration mode. A 30-hp, 118-Nm, 1800-rpm IPMSM manufactured by Marathon Electric [14] is modeled in Simulink and fed through a three-phase, 480V, 60-Hz AC grid. The motor is assumed to be directly coupled to a wire drum of 0.5-m diameter to lift and lower a100-N weight through a 300-m-deep abandoned well. The IPMSM drive is fed through a back-to-back PWM inverter system that constitutes the power electronics system of the electromechanical system in the GESS, such as the one illustrated in Fig. 2.

To simplify the analysis, we do not consider the gearbox and the hydrodynamic interactions between the fluid and the weight. The shaft speed is used to decipher the position of the weight. The control system optimizes round-trip efficiency during ascent and descent.

The power electronics system comprises a PWM converter and an IPMSM drive. The PWM converter comprises a boost inductor connected in series with the grid and a grid-side converter that converts AC power from the grid into DC power for the IPMSM drive during charging. The inductor serves to filter the voltage harmonics at the midpoint of each phase leg of the grid-side converter. In addition, the inductor limits the harmonic distortion in the line current.

The IPMSM drive comprises a load-side converter connected to an IPMSM. The switching of this converter is controlled using a Field-Oriented-Control (FOC) to deliver the load torque at the reference speed. The FOC is a widely recognized technique for controlling electric machines in all the possible modes of operation, such as motoring, braking, and reverse motoring. Its underlying principle involves separating the current into two quadrature components: one responsible for generating magnetic flux (I_d) and another for producing torque (I_q). This decoupling enables independent control over these two quadrature current components. A comparable approach is adopted for controlling PWM converters. By decoupling the grid current, it is possible to independently control the active component (which supplies the load current and regulates the DC link voltage) and the reactive component. In addition, the FOC ensures smooth power conversion, meets IEEE and IEC standards, minimizes losses, and enhances power quality. Therefore, the FOC is used to control both the grid side and motor side converters, which is explained in the following section.

3. Control and Operation of PWM Converter Feeding the IPMSM Drive

The PWM converter feeding the IPMSM drive enables the following features:

1. *Four quadrant operation:* The PWM converter enables power flow in both directions, allowing charging from the grid and regenerative operation during discharging.
2. *Voltage sag compensation:* The boost rectifier mode ensures a constant DC link voltage, maintaining system operation even during grid voltage fluctuations.
3. *Controlled power factor:* The PWM converter maintains a unity power factor by adjusting the load-side converter to meet the motor's reactive power demand, enabling efficient power transfer between the grid and DC link.

Assuming a typical motor efficiency (η_m) as 95%, and the efficiency of the grid-side converter (η_g) as 98%, the required DC power (P_{DC}) and grid-side power (P_{grid}) are expressed as:

$$P_{DC} = V_{DC} I_{DC} = \frac{P_{motor}}{\eta_m} = 23.56\ kW \tag{3}$$

$$P_{grid} = \frac{P_{DC}}{\eta_g} = 24.04\ kW. \tag{4}$$

Notably, the DC link voltage synthesizes a PWM voltage at the three-phase terminal of the grid-side converter. To ensure sinusoidal PWM voltage (V_{inv}), the DC link voltage must satisfy (5) [16]:

$$V_{DC} \geq 2\sqrt{2} V_g \tag{5}$$

where V_g is the AC grid phase voltage. Thus, in the following analysis, the phase voltage is maintained at 785V. For a linear continuous PWM scheme, the grid-side converter phase voltage (V_{inv}) can be expressed as [15]:

$$V_{inv} = \frac{m V_{DC}}{2\sqrt{2}}, \tag{6}$$

where m is the modulation index. Herein, to ensure lower current and voltage harmonics, a space-vector PWM (SVPWM) scheme is used. Thus, the maximum possible modulation index is 1.15. However, to ensure a sufficient pulse width, the modulation index is limited to 1. Therefore, using (6), the grid-side converter voltage is 481V. To achieve unity power factor at the grid, the grid voltage and the current must be co-phasal. The phasor diagram representing the relation between the grid voltage and the grid-side converter voltage (V_{inv}) is illustrated in Fig. 3, wherein the grid-side converter voltage is larger and lags the grid voltage. According to the

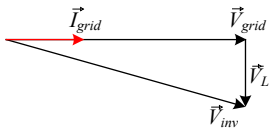

Fig. 3. Phasor diagram of PWM converter under operation.

phasor diagram, the inductance (L) is

$$L = \frac{1}{\omega I_{grid}}\sqrt{V_{grid}^2 + V_{inv}^2}, \tag{7}$$

where I_{grid} is the rated grid current. Using (7), the inductance is 1.71 mH.

The capacitance (C_{DC}) of the capacitor at the DC link depends on the permissible ripple voltage (ΔV_{DC}). If the peak-to-peak permissible ripple voltage is 5%, then the DC link capacitance is computed using (8) as [15]:

$$C_{DC} \geq \frac{mI_{grid}}{4\omega\Delta V_{DC}}. \tag{8}$$

Thus, the DC link capacitance in this analysis is 1 mF.

3.1 Field-Oriented Control (FOC)

In FOC, the three-phase voltage and current (V_a, V_b, V_c and I_a, I_b, I_c) are transformed into a two-phase equivalent system (V_α, V_β and I_α, I_β) using a Clarke transformation [17], also called a stationary reference frame. These quantities are further transformed into synchronously rotating reference frames (V_d, V_q and I_d, I_q) using a Park transformation [17], which rotates at grid frequency (ω). The Clarke and Park voltage transformations can be expressed as [15]:

$$\begin{bmatrix} V_\alpha \\ V_\beta \end{bmatrix} = \begin{bmatrix} 1 & -\frac{1}{2} & -\frac{1}{2} \\ 0 & \frac{\sqrt{3}}{2} & -\frac{\sqrt{3}}{2} \end{bmatrix} \begin{bmatrix} V_a \\ V_b \\ V_c \end{bmatrix} \tag{9a}$$

$$\begin{bmatrix} V_d \\ V_q \end{bmatrix} = \begin{bmatrix} cos\theta & sin\theta \\ -sin\theta & cos\theta \end{bmatrix} \begin{bmatrix} V_\alpha \\ V_\beta \end{bmatrix}, \tag{9b}$$

where θ is the angle between the stationary phase "a" axis and the synchronously rotating "d" axis. The major difference between the control of the PWM converter and the IPMSM drives lies in the alignment of the "d" axis when $\omega t = 0$, which is defined by the angle θ.

3.1.1 Field-Oriented Control of PWM Converter

In the FOC of the PWM converter, to reduce the variables in control, we assume that the voltage phasor aligns with the "q" axis, which implies that at $\omega t = 0$, the "d" axis aligns with the "a" axis, and the "d" axis component of the grid voltage is 0. This simplifies the voltage equation in the synchronously rotating frame which can now be expressed as [16]:

$$Ri_{gd} + L\frac{di_{gd}}{dt} - \omega Li_{gq} + v_{id} = v_{gd} = 0 \tag{10a}$$

$$Ri_{gq} + L\frac{di_{gq}}{dt} + \omega Li_{gd} + v_{iq} = v_{gq}, \tag{10b}$$

where R and L are the resistance and the inductance of the line inductor, i_{gd} and i_{gq} are the "d" and "q" axis grid current, ω is the angular frequency, v_{gd} and v_{gq} are the "d" and "q" axis grid voltage, and the v_{id} and v_{iq} are the "d" and "q" axis components of the grid-side converter voltage (V_{inv}).

A schematic of the PWM converter FOC is shown in Fig. 4 (largely adapted from [15]). First, a phase-locked loop (PLL) is used to compute the angle θ[15]. Thereafter, the grid voltage and current are transformed into "d" and "q" axis components using (9), and these components are used as feedback terms for the controllers. Then, the error in the DC link voltage ($e_{DC} = V_{DC}^* - V_{DC}$) is fed to the voltage controller (G_v), which is expressed mathematically as [18]:

$$G_v = \frac{K_v(1+sT_v)}{sT_v}, \tag{11}$$

where K_v is the proportional gain and T_v is the integrator time constant. The controller generates a reference signal for the "q" axis current (i_{gq}^*). For unity power factor operation, the grid voltage and currents must be co-phasal. Hence, the "d" axis reference current (i_{gd}^*) is set to 0. The errors in the "d" and "q" axis currents ($e_d = i_{gd}^* - i_{gd};\ e_q = i_{gq}^* - i_{gq}$) are fed to the current controller (G_c) as [16]:

$$G_c = \frac{K_c(1+sT_c)}{sT_c}, \tag{12}$$

where K_c is the proportional gain and T_c is the integrator time constant. The controller generates reference signals for the "d" and "q" axis grid-side converter voltages (v_{id}^*, v_{iq}^*). According to equations (10a) and (10b), cross-coupling terms exist in the "d" and "q" axis voltage equations. Thus, for their independent control, the feedforward terms v_{dff} and v_{qff} must be added to the controller output to generate the final "d" and "q" axis voltages (v_d^*, v_q^*). This is illustrated in Fig. 4 and is expressed mathematically as [16]:

$$v_d^* = \frac{1}{K_a}\left(-\left(\underbrace{Ri_{gd} + L\frac{di_{gd}}{dt}}_{v_{id}^*}\right) + \underbrace{\omega Li_{gq}}_{v_{dff}}\right) \tag{13a}$$

$$v_q^* = \frac{1}{K_a}\left(-\left(\underbrace{Ri_{gq} + L\frac{di_{gq}}{dt}}_{v_{iq}^*}\right) - \underbrace{\omega Li_{gd}}_{v_{qff}}\right), \tag{13b}$$

where v_{dff} and v_{qff} are the feedforward terms of "d" and "q" and K_a is the converter gain with the time constant T_a. The dynamics of the voltage and current sensors are represented as a first-order system with gains K_1 and K_2, respectively, and time constants T_1 and T_2, respectively. In the synchronously rotating frame, the active and reactive power (P_{grid}, Q_{grid}) fed by the grid are expressed mathematically as:

$$P_{grid} = \frac{2}{3}\left(v_{gq}i_{gq} + v_{gd}i_{gd}\right) = \frac{2}{3}\left(v_{gq}i_{gq}\right) \tag{14a}$$

$$Q_{grid} = \frac{2}{3}\left(v_{gq}i_{gd} - v_{gd}i_{gq}\right) = \frac{2}{3}\left(v_{gq}i_{gd}\right). \tag{14b}$$

For unity power factor operation, as the reactive power input from the grid is zero, the "d" axis current reference (i_{gd}^*) is set to 0. Using equations (3) and (14a), the power balance constant (K) is defined as [16]:

$$Ki_{gq} = I_{DC} = \frac{2}{3}\eta_m\frac{v_{gq}i_{gq}}{V_{DC}}. \tag{15}$$

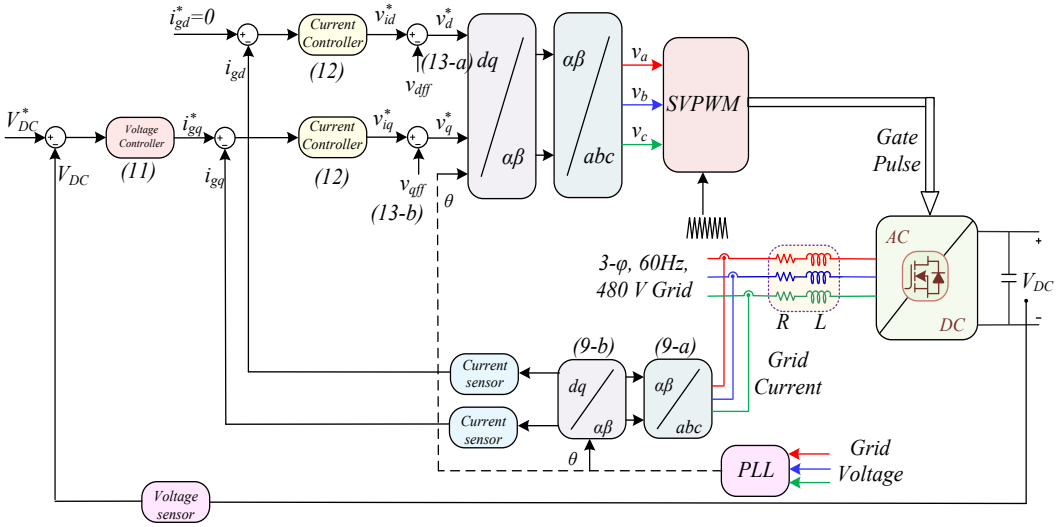

Fig. 4. Field-oriented control of PWM converter.

The parameters of the controllers are tuned according to [16].

3.1.2 Field-Oriented Control of IPMSM

The FOC of the IPMSM is like the FOC of the PWM converter, except for the following:

1 *Alignment of synchronously rotating frame*: The synchronously rotating frame is synchronised to the rotor position (measured using the encoder) such that the "*d*" axis is aligned with the magnet flux. Therefore, unlike the PWM converter, the "*d*" axis motor voltage (v_{md}^*) is nonzero.

2 *Reluctance torque*: A "*d*" axis current is injected into the IPMSM to harness the advantages of the reluctance torque [17]. Therefore, unlike the PWM converter, the reference signal for the "*d*" axis current (i_{md}^*) is nonzero. The "*d*" and "*q*" axis reference currents are generated using Maximum Torque Per Ampere (MTPA) control [17], which is discussed in Section 3.1.2.1. The MTPA approach is used to obtain the minimum current space vector for a constant torque trajectory, resulting in minimal losses and maximum efficiency.

Akin to the FOC of the PWM inverter, the "*d*" and "*q*" axis currents of the motor are controlled independently to achieve the reference speed at a given load torque. The "*d*" and "*q*" axis voltages can be expressed as [18]:

$$R_s i_{md} + L_d \frac{di_{md}}{dt} - \omega_e L_q i_{mq} = v_{md} \tag{16a}$$

$$R_s i_{mq} + L_q \frac{di_{mq}}{dt} + \omega_e L_d i_{md} + \omega_e \psi_m = v_{mq}, \tag{16b}$$

where R_s is the stator winding resistance, L_d and L_q are the "*d*" and "*q*" axis inductances, ω_e is the electrical speed of the synchronously rotating frame, ψ_m is the peak flux linkage, and v_{md} and v_{mq} and i_{md} and i_{mq} are the "*d*" and "*q*" axis voltages and the phase currents, respectively. The electrical speed is related to the mechanical shaft speed (ω_m) as:

$$\omega_e = P\omega_m \tag{17}$$

where P is the number of pole pairs. The electromagnetic torque (τ_d) developed by the machine depends on both the "*d*" and "*q*" axis currents, and is expressed as [15]:

$$\tau_d = \frac{3}{2} P\left(\psi_m i_{mq} + \left(L_d - L_q\right) i_{md} i_{mq}\right). \tag{18}$$

The first term in (18) represents the torque due to flux linkage, whereas the second term represents the reluctance torque, which arises due to the difference in the inductance between the "*d*" and "*q*" axes. Because $L_d < L_q$ for IPMSM, the torque can be increased by injecting negative "*d*" axis current.

A schematic of the FOC of the PWM inverter is given in Fig. 5. Akin to the FOC of the PWM converter, the error in the machine speed ($e_\omega = \omega_m^* - \omega_m$) is fed to the speed controller (G_ω), which is expressed as [16]:

$$\mathrm{G}_\omega = \frac{K_\omega(1+sT_\omega)}{sT_\omega}, \tag{19}$$

where K_ω is the proportional gain and T_ω is the integrator time. The controller generates a reference signal for the electromagnetic torque (τ_d^*). This refence torque is used in the MTPA control to generate the "*d*" and "*q*" axis current references (i_d^* and i_q^*), which are discussed in Section 1.2.1. The errors in the "*d*" and "*q*" axis currents ($e_d = i_d^* - i_d$; $e_q = i_q^* - i_q$) are fed to the current controller (G_c^m), which is expressed mathematically as [16]:

$$G_c^m = \frac{K_c^m(1+sT_c^m)}{sT_c^m}, \tag{20}$$

where K_c^m is the proportional gain and T_c^m is the integrator time. This controller generates reference signals for the "*d*" and "*q*" axis voltages (v_{id}^*, v_{iq}^*). According to (16), cross-coupling terms exist in the "*d*" and "*q*" axis voltage equations.

Thus, for independent control of the "*d*" and "*q*" axis currents, feedforward terms (v_{dff}, v_{qff}) must be added to the controller output to generate the "*d*" and "*q*" axis voltages (v_d^*, v_q^*). This is illustrated in Fig. 5 and is expressed as [18]:

$$v_d^* = \frac{1}{K_a^m}\left(\underbrace{R_s i_{md} + L_d \frac{di_{md}}{dt}}_{v_{id}^*} - \underbrace{\omega_e L_q i_{mq}}_{v_{dff}}\right) \tag{21a}$$

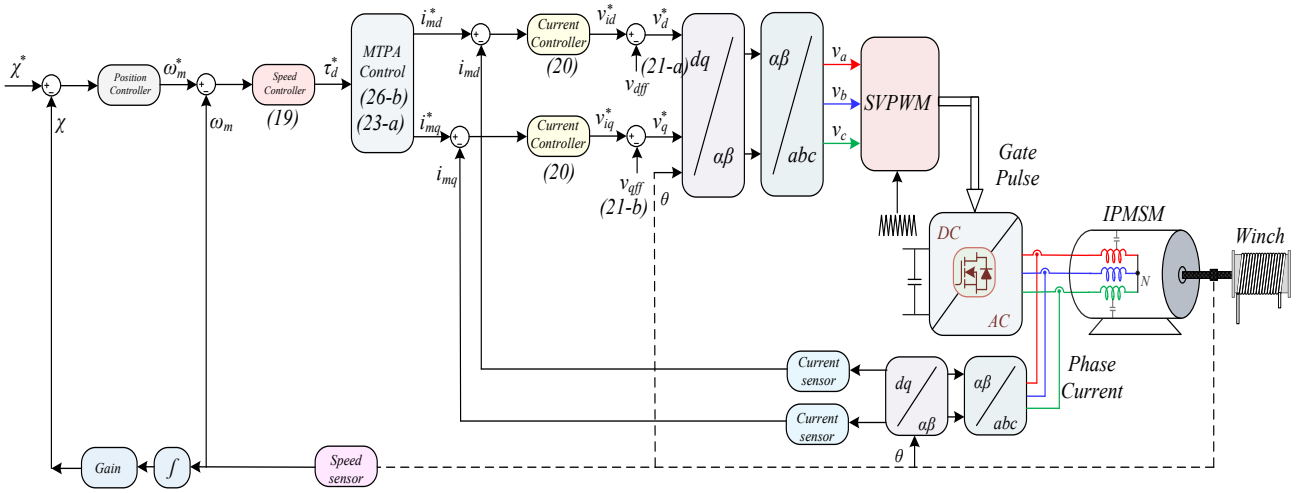

Fig. 5. Field-oriented control of IPMSM with maximum torque per ampere control.

$$v_q^* = \frac{1}{K_a^m}\left(\underbrace{Ri_{mq} + L\frac{di_{mq}}{dt}}_{v_{iq}^*} + \underbrace{\omega_e L_d i_{md} + \omega_e \psi_m}_{v_{qff}}\right) \quad (21b)$$

where, v_{dff} and v_{qff} are the feedforward terms of "d" and "q" and K_a^m is the converter gain with time constant T_a^m. The dynamics of the speed and current sensors are represented as a first-order system with gains K_1^m and K_2^m, and time constants T_1^m and T_2^m, respectively. The parameters of the controllers, converters, and sensors are evaluated according to [18].

The inertia (J_s) and friction coefficient (B) of the shaft represent a first-order system that is used to deduce the relationship between the electromagnetic torque (τ_d) and the load torque (τ_l):

$$\omega_m = \frac{\tau_d - \tau_l}{(Js+B)}. \quad (22)$$

3.1.2.1 Maximum Torque per Ampere (MTPA) Control

Using equation (18), the torque can be maximized by injecting a negative "d" axis current, which is quantified using MTPA control [17]. Using (18), the electromagnetic torque can be expressed in per-unit (p.u) as [17]:

$$\tau_d^{p.u} = i_q^{p.u}\left(1 - i_d^{p.u}\right), \quad (23a)$$

where $\tau_d^{p.u}$, $i_d^{p.u}$, and $i_q^{p.u}$ are the per-unit torque and the "d" and "q" axis currents, respectively. The base values of the torque and current are $\tau_{d_{base}}$ and i_{base}, respectively, which are expressed mathematically using [17] as:

$$i_{base} = -\frac{\psi_m}{(L_d - L_q)} \quad (24a)$$

$$\tau_{base} = \frac{3}{2} P \psi_m i_{base} \quad (24b)$$

For the MTPA control, the minimum current space vector for constant torque is obtained when the "d" and "q" axis currents satisfy the following relation [17]:

$$\frac{\partial\left(\tau_d/i_s\right)}{\partial i_d} = 0 \quad (25a)$$

$$\frac{\partial\left(\tau_d/i_s\right)}{\partial i_q} = 0, \quad (25b)$$

where i_s the stator current magnitude, which is expressed as $i_s = \sqrt{i_d^2 + i_q^2}$. Using (18) and (23–25), the per-unit torque can be deduced as [17]:

$$\tau_d^{pu} = \sqrt{-i_d^{pu}.\left(1 - i_d^{p.u}\right)^3} \quad (26a)$$

$$\tau_d^{pu} = \frac{1}{2} i_q^{pu}\left(1 + \sqrt{1 + 4 i_q^{p.u\,2}}\right). \quad (26b)$$

The reference "d" and "q" axis currents can be estimated using (26). However, (26) is a nonlinear equation. Therefore, the reference "d" and "q" axis currents are estimated using a lookup table. We assume that during normal operation, the "d" and "q" axis currents are within 3 p.u. Using (26b), we calculate the per-unit torque by varying the $i_q^{p.u}$ between 0 and 3. Using (23a) and the calculated torque, we calculate $i_d^{p.u}$. The calculated $i_d^{p.u}$ and $i_q^{p.u}$ and the torque form a lookup table, which is used to estimate the "d" and "q" axis currents for a given reference torque. The reference torque is generated by the speed controller. Importantly, this approach is quicker, and it is based on a lookup table that is derived from only two equations, (23a) and (26b). In addition, this method is general enough to be applicable to any IPMSM, regardless of specific motor parameters, owing to the per-unit conversion.

4. Results and Discussion

The control of the IPMSM drive fed through a PWM converter is implemented and verified using a MATLAB simulation. A MATLAB/Simulink model is used to evaluate the dynamic and steady-state performance along with the round-trip efficiency. For the simulation, a standard weight of 100 N is raised from a well of depth 300 m, which represents the charging mode. The weight descends to represent the discharging mode. The ground is marked as 0 m and the bottom of the well is marked as −300 m. Fig. 6(a) shows the plots for the load torque, developed electromagnetic torque, shaft speed, and reference speed during both charging and discharging modes. The actual depth of the weight follows the reference depth without overshoot, which is mainly due to the overdamped response of the position controller (G_P)

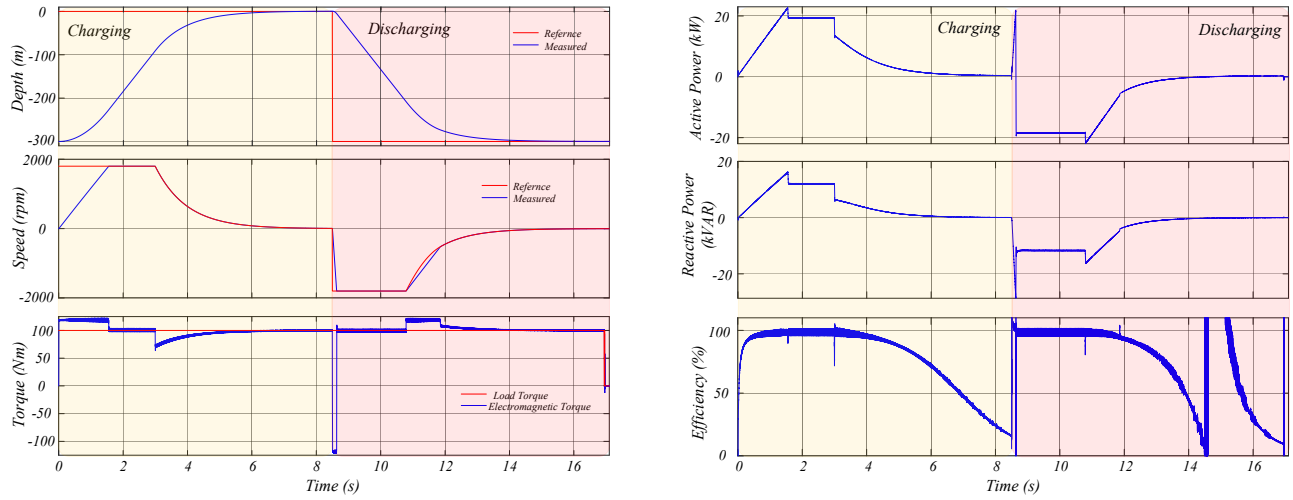

(a) (b)

Fig. 6. Performance of the GESS. (a) Depth, speed, and torque developed by the IPMSM; (b) active and reactive power consumed by the IPMSM, and the efficiency of the motor.

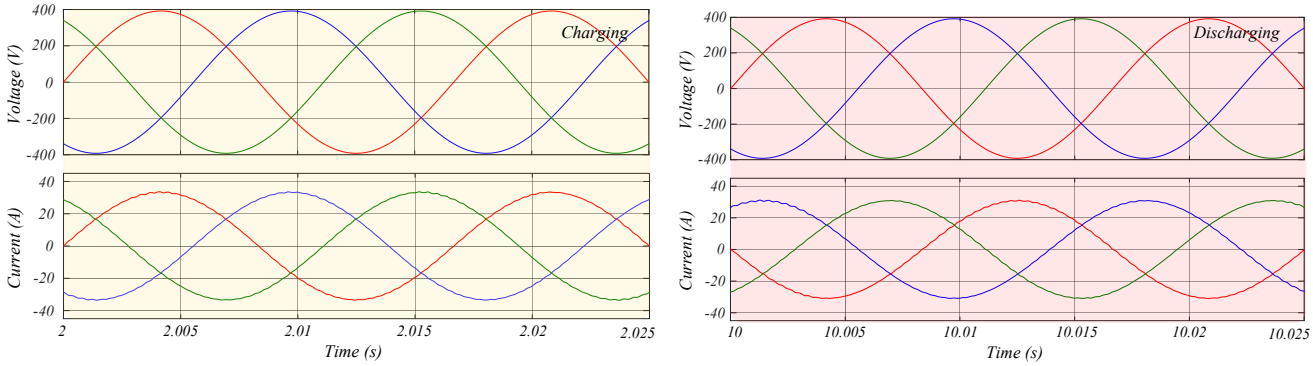

(a) (b)

Fig. 7. Grid voltage and current during the charging and discharging operation.

In addition, the shaft speed follows the reference speed without a sluggish response. During acceleration and deceleration, the machine develops rated electromagnetic torque (118 Nm) to provide sufficient torque. During this transient, the acceleration and deceleration are governed by the shaft characteristics (22).

Fig. 6(b) illustrates the active and reactive power consumed by the machine along with its efficiency. The positive power represents the motoring mode of operation, whereas the negative power represents the regenerating mode. The machine consumes peak-rated power during acceleration and deceleration. When the weight is raised, the machine consumes electrical power and transforms it into mechanical power. When the weight reaches the surface, the position controller acts to reduce the speed by adjusting the speed reference. At lower speeds, the machine efficiency drops abruptly from 95% to 20%. A similar trend was observed during the discharging operation. During discharging, the weight descends to the bottom of the well. As the weight descends, the machine operates as a generator and delivers electrical power from the stored mechanical energy at 95% efficiency. When the weight reaches the bottom of the well (i.e., the reference depth), the position controller acts to reduce the speed, and the machine speed decreases, resulting in an abrupt decrease in machine efficiency. This is intuitive because the speed-dependent losses in the machine are greater at lower speeds. The grid voltage and the current during the charging and discharging operation are shown in Fig. 7. As is illustrated, the current is sinusoidal and is in phase with the voltage. The current total harmonic distortion is less than 5%, which adheres to the IEEE 1547-2018 [3] and IEC TS 62786:2017 [4] standards. Also, the power factor at the grid-side is maintained unity during both modes of operation. This is further validated by Fig. 8, which illustrates the active and reactive power delivered and consumed by the grid along with the efficiency of the driveline.

The efficiency at the grid side is calculated as the ratio of

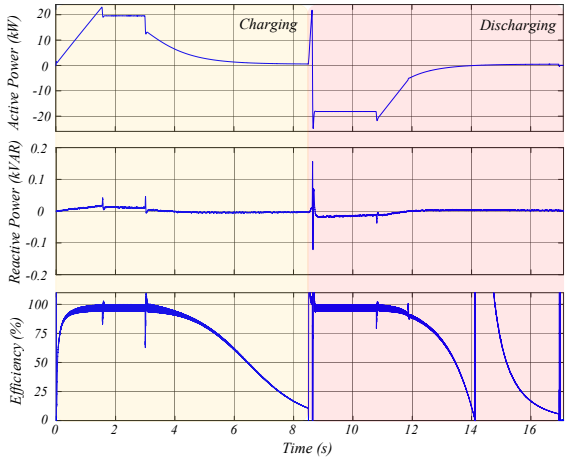

Fig. 8. Active and reactive power delivered by the grid and the efficiency of the driveline during a round trip.

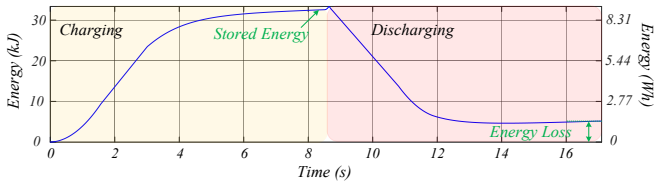

Fig. 9. Energy delivered by the grid during a round trip.

the mechanical power output at the shaft to the active power measured at the grid. During both modes of operation, the reactive power consumption is 0 kVAR, which confirms the unity power factor operation of the grid. Also, the overall efficiency of the drivetrain follows the motor efficiency, which indicates that the major losses occur within the electric machine and can be improved by opting for a high-efficiency motor. Notably, only the conduction losses within the converters are considered, which is represented by the "ON" state voltage drop across the semiconductor devices.

Fig. 9 shows the energy stored and delivered by the grid during charging and discharging; this energy is the integration of the grid active power. During the charging cycle, the energy delivered by the grid increases. The total potential energy stored during the charging cycle is 32.5 kJ, which is represented as the energy at the end of the charging cycle. During the discharging cycle, the energy decreases as the stored mechanical energy is delivered back to the grid. The energy at the end of the cycle represents the energy loss, which is 4.58 kJ. The efficiency of the GESS during charging is 92.3%, which is calculated as the ratio of the potential energy of the weight to the energy supplied by the gid. By contrast, the efficiency during the discharging process is 84.73%, which is due to low-speed operation over a long period.

The round-trip efficiency for the modeled system is 85.9%. However, the losses in the mechanical system (comprising the winch and the gearbox) were not considered. In addition, the efficiency can be improved when the stored energy increases. This can be achieved by increasing the weight or increasing the duration of acceleration and deceleration (e.g., possible by making use of a deeper well).

5. Conclusion

In this analysis, we develop control and operation of a power electronics system for the RIGS-UP GESS application. A dynamic MATLAB/Simulink model evaluates the behaviour of a 30-hp IPSM-based drivetrain system. Results indicate a round-trip efficiency of up to 85.9% solely from the electrical system when storing 65 kJ of energy. The major losses occur when the machine is operating at near-zero speed, resulting in lower efficiency. The maximum efficiency occurs during acceleration and deceleration. Therefore, the efficiency can be maximized by increasing the ascent/descent time. This can be achieved by utilizing a deeper well or by using a gearbox with a greater speed reduction ratio that will increase the duration of ascent/descent of the weight. However, using a gearbox may incur additional mechanical losses.

Acknowledgement

The authors would like to acknowledge the support and input for the drive system modelling from project partners Stefan Streckfus and Kemp Gregory from Renewell Inc. This work was authored by the National Renewable Energy Laboratory, operated by Alliance for Sustainable Energy, LLC, for the U.S. Department of Energy (DOE) under Contract No. DE-AC36-08GO28308. The funding was provided by the Advanced Research Projects Agency – Energy (ARPA-E), U.S. Department of Energy under the grant CX-026130: "Repurposing Infrastructure for Gravity Storage Using Underground Potential Energy (RIGS-UP)". The views and opinions of authors expressed herein do not necessarily state or reflect those of the United States Government or any agency thereof. The U.S. Government retains and the publisher, by accepting the article for publication, acknowledges that the U.S. Government retains a nonexclusive, paid-up, irrevocable, worldwide license to publish or reproduce the published form of this work, or allow others to do so, for U.S. Government purposes.

References

[1] G. Ozin, "Gravity energy storage elevated to new heights", April 2022, [Online], available https://www.advancedsciencenews.com/gravity-energy-storage-elevated-to-new-heights/, accessed 18 June 2023.

[2] "Ideal and orphaned oil and gas wells: State and provincial regulatory strategies", *Interstate oil and gas compact commission (IOGCC)*, 2021.

[3] IEEE Standard for Interconnection and Interoperability of Distributed Energy Resources with Associated Electric Power Systems Interfaces, IEEE-1547, 2018.

[4] Distributed energy resources connection with the grid, IEC TS 62786:2017.

[5] C.D. Botha, M.J. Kamper, "Capability study of dry gravity energy storage", *J. Energy Storage*, vol. 23, pp. 159–174, 2019.

[6] A. C. Ruoso, N. R. Caetano, L. A. O. Rocha, "Storage gravitational energy for small scale industrial and residential applications", *Inventions,* vol. 64, no. 4, 2019.

[7] W. Tong, Z. Lu, H. Zhao, et al., "The structure and control strategies of hybrid solid gravity energy storage system", *Journal of Energy. Storage*, vol. 67, 2023.

[8] O. K. Bowoto, O. P. Emenuvwe, M. N. Azadani, "Gravitricity based on solar and gravity energy storage for residential applications", *Int. J. Energy Environ. Eng.*, vol. 12, pp. 503–516, 2021.

[9] Blair, C., "Gravitricity technology", Gravitricity, [Online], available: https://gravitricity.com/technology/, accessed 14 June 2023.

[10] Gravity Power, [Online], available: https://www.gravitypower.net, Accessed 14 June 2023.

[11] K. Loudiyi, A. Berrada, "Experimental validation of gravity energy storage hydraulic modeling", *Energy Proc.*, vol. 134, pp. 845–854, 2017.

[12] Jaquez P. V., "Converting oil and gas wells to energy storage", Renewell, [Online], available: https://renewellenergy.com/wp-content/uploads/2022/11/P1-Converting-Wells-to-Energy-Storage-Renewell-Energy-1.pdf, accessed 14 June 2023.

[13] ARPA-E Project: "Repurposing Infrastructure for Gravity Storage using Underground Potential energy (RIGS UP), 2021", available: https://www.energy.gov/nepa/articles/cx-026130-national-renewable-energy-laboratory-rigs-repurposing-infrastructure, accessed 14 June 2023.

[14] Datasheets, Marathon Electric, pp. 1 [Online], available: https://www.regalrexnord.com/products/electric-motors/ac-motors-nema/permanent-magnet-pmac-motors/permanent-magnet-pmac-motor-30-hp-3-ph-120-hz-460-v-1800-rpm-286tc-frame-tefc-286tpfsa10090, accessed 14 June 2023.

[15] Bimal K. Bose, "Modern power electronics and AC drives", *1st ed.*, Upper Saddle River, New Jersey, Prentice Hall PTR, Prentice-Hall, Inc., 2002.

[16] Siva Prasad, J.S., Bhavsar, T., Ghosh, R. et al. "Vector control of three-phase AC/DC front-end converter", *Sadhana*, 33, pp. 591–613, May 2009.